Meteorology and Atmospheric Physics (2019) 131:431–441
https://doi.org/10.1007/s00703-018-0581-x

ORIGINAL PAPER

The chemical effects on the summertime ozone in the upper troposphere and lower stratosphere over the Tibetan Plateau and the South Asian monsoon region

Yixuan Gu[1] · Hong Liao[2] · Jianming Xu[1] · Guangqiang Zhou[1]

Received: 20 October 2017 / Accepted: 19 January 2018 / Published online: 31 January 2018

Abstract
We use the global three-dimensional Goddard Earth Observing System chemical transport model with the Universal tropospheric–stratospheric Chemistry eXtension mechanism to examine the contributions of the chemical processes to summertime O_3 in the upper troposphere and lower stratosphere (UTLS) over the Tibetan Plateau and the South Asian monsoon region (TP/SASM). Simulated UTLS O_3 concentrations are evaluated by comparisons with Microwave Limb Sounder products and net chemical production of O_3 (NP_{O3}) are evaluated by comparisons with model results in previous studies. Simulations show that the chemical processes lead to an increase in O_3 concentration, which is opposite to the effect of O_3 transport in the UTLS over the TP/SASM region throughout the boreal summer. NP_{O3} in UTLS over the TP/SASM region is the largest in summer. Elevated values (0.016–0.020 Tg year^{-1}) of the seasonal mean NP_{O3} are simulated to locate at 100 hPa in the TP/SASM region, where the mixing ratios of O_3 are low and those of O_3 precursors (NO_x, VOCs, and CO) are high. The high concentrations of O_3 precursors (NO_x, VOCs, and CO) together with the active photochemical reactions of NO_2 in the UTLS over the TP/SASM region during summertime could be important reasons for the enhancement of NP_{O_3} over the studied region.

1 Introduction

Ozone (O_3) is an important gas constituent in the atmosphere. Tropospheric O_3 is not only a vital air pollutant that has adverse effects on human health (Fann et al. 2012) and ecosystems (Shindell et al. 2012; Yue and Unger 2014) but also acts as a greenhouse gas with global mean radiative forcing of 0.4 W m^{-2} (Alexander et al. 2007). Stratospheric O_3 accounts for about 90% of the O_3 on the earth, concentrating at altitudes between 10–30 km and shielding the plants and animals from harmful solar radiation (McConnell and Jin 2008). In combination with molecules, such as methane and water vapor, O_3 is a major source of OH radical which acts as a detergent for many chemical species (Seinfeld and Pandis 2006). Affected by both the anthropogenic emissions and the stratospheric–troposphere (STE), O_3 in the upper troposphere and lower stratosphere (UTLS) shows distinctive regional characteristics and has drawn growing attention over the past few years (Oltmans et al. 1998; Logan et al. 1999; Staehelin et al. 2001; Rao et al. 2003; Bian et al. 2011).

Both the observational and modeling studies have shown that the summertime O_3 level in UTLS over the Tibetan Plateau (TP) and the South Asian summer monsoon (SASM) region is much lower than that of other areas at the same altitudes (Fu et al. 2006; Randel and Park 2006; Bian et al. 2011; Gu et al. 2016). Bian et al. (2011) examined satellite measurements from Microwave Limb Sounder (MLS) products and reported the presence of a low-ozone area at 100 hPa over the Asian summer monsoon region, corresponding to the South Asian High, in summer during 2005–2009. Based on the MLS measurements and the Goddard Earth Observing System chemical transport model (GEOS-Chem) simulations, Gu et al. (2016) reported that the relatively low O_3 concentrations of less than 200 ppbv were located at 100 hPa within the Asian anticyclone region

Responsible Editor: S. Trini Castelli.

✉ Hong Liao
hongliao@nuist.edu.cn

[1] Yangtze River Delta Center for Environmental Meteorology Prediction and Warning, Shanghai 200030, China

[2] School of Environmental Science and Engineering, Nanjing University of Information Science and Technology, Nanjing 210044, China

during summer of 2005. Previous studies suggested that the summertime low-ozone area in UTLS is caused by the dynamics over TP and the Asian summer monsoon (Gettelman et al. 2004; Zhou et al. 2006; Tian et al. 2008; Tobo et al. 2008). TP/SASM region is a vital pathway of mass exchange between the troposphere and stratosphere because of the frequent deep convections during the boreal summer. The deep convections associated with the Asian summer monsoon transport the ozone-poor air from the boundary layer into the UTLS, and the upper-level Tibetan anticyclone in the UTLS acts to isolate air and traps the uplifted air within the anticyclone region (Gettelman et al. 2004; Fu et al. 2006; Bian et al. 2011).

Though the summertime ozone valley in the UTLS over TP has been widely discussed in the past few years, few studies have investigated the role of chemical processes in the formation of the low ozone region over the TP/SASM in boreal summer. Liu et al. (2003) calculated the physical and chemical contributions to the changes in the mean O_3 concentration at a selected grid point (31°N, 90°E, 100 hPa) from April to July using the OSLO CTM2 model. They reported that the effect of the chemical process on the mean O_3 concentration at that point is 87.7 ppbv at 100 hPa during April to July, which is opposite to that of the dynamic process (− 49.7 ppbv) and cannot be neglected. Although Liu et al. (2003) provided valuable knowledge regarding the chemical effects on summertime O_3 in UTLS, more investigation is needed. First, the calculation of Liu et al. (2003) was focused on one specific point, and the regional characteristics of the chemical contributions were not included; Second, the corresponding reasons for the positive chemical contributions over the TP/SASM regions, such as the related chemical processes, were not systematically discussed; third, the chemistry of the OSLO CTM2 model used in Liu et al. (2003) was only valid for the troposphere, which was limited in the study of chemistry process over the UTLS region. TP is surrounded by large anthropogenic emission sources such as India, Southeast Asia, and southern China (Li et al. 2005; Lau et al. 2006). Pollutants from these places can be transported to TP by prevailing winds in the monsoon seasons (Lawrence and Lelieveld 2010; Xia et al. 2011), and then be uplifted to the UTLS through deep convections (Li et al. 2005; Randel et al. 2010). Anthropogenic emissions together with the unique dynamic characteristics of TP result in persistent maxima of O_3 precursors (e.g. CO, NO_x, C_2H_6) locating in the UTLS over the TP/SASM region during summertime (Kar et al. 2004; Park et al. 2004a, 2008; Li et al. 2005). The investigation of the chemical effects on the summertime O_3 in the UTLS not only provides further information on the formation of the summertime low O_3 concentration in UTLS over the TP/SASM region, but also offers insight into the influence of human activities on O_3 in the UTLS over the TP/SASM region in boreal summer.

This work aims to give a comprehensive view of the effects of the chemical processes on summertime O_3 in UTLS over TP/SASM (10–40°N, 70–105°E) using the global Goddard Earth Observing System chemical transport model (GEOS-Chem) driven by the assimilated meteorological fields. A brief description of the GEOS-Chem model and numerical experiment is presented in Sect. 2. Section 3 evaluates the model's performance for O_3 concentrations in different seasons. Section 4 shows the simulated chemical contributions to the UTLS O_3 over the TP/SASM region in summer. Section 5 discusses the corresponding reasons for the regional characteristics of O_3 chemical productions over the TP/SASM region in summer.

2 Model description and numerical experiment

2.1 Model description

We simulate the UTLS O_3 using the global chemical transport model GEOS-Chem (version 11-01, http://geos-chem.org) with the Universal tropospheric–stratospheric Chemistry eXtension (UCX) mechanism. For the simulations presented in this paper, we use the GEOS-5 assimilated meteorological fields from the Goddard Earth Observing System of the NASA Global Modeling and Assimilation Office. The model used here has a horizontal resolution of 2° latitude by 2.5° longitude and 72 hybrid sigma-eta pressure layers extending from the surface to 0.01 hPa. Over the TP/SASM region, the model has about 35 layers in the troposphere and 25 layers in the stratosphere.

The Geos-Chem model includes a detailed treatment of tropospheric O_3–NO_x–hydrocarbon and aerosol chemistry. The aerosol species include sulfate, nitrate, ammonium (Park et al. 2004b; Pye et al. 2009), organic carbon, black carbon (Park et al. 2004b), mineral dust (Fairlie et al. 2007), and sea salt (Alexander et al. 2005; Jaeglé et al. 2011). Tropospheric O_3 chemistry includes about 80 species and over 300 chemical reactions (Bey et al. 2001). The photolysis and UV transfer in the model is calculated using the Fast-JX v7.0a model (Wild et al. 2000; Eastham et al. 2014) in 18 wavelength bins covering 177–850 nm. The gas–aerosol partitioning of nitric acid and ammonium is calculated using the ISORROPIA II thermodynamic equilibrium module (Fountoukis and Nenes 2007).

The UCX extends the chemistry mechanism in the model to include reactions relevant to the stratosphere (Eastham et al. 2014). The extended model includes 132 chemical species, with long-lives species such as N_2O, CH_4, OCS, and CFCs. The heterogeneous reactions and photolytic decompositions in the stratosphere are identified by comparing reactions and processes in the GMI stratospheric chemistry

mechanism (Rotman et al. 2001). The reaction constants are updated according to JPL 10-06 (Sander et al. 2011). The Fast-JX includes cross-section data for species relevant to both the troposphere and the stratosphere.

The convective transport in GEOS-Chem imitates that in the parent GEOS general circulation model (Hack 1994; Zhang and McFarlane 1995), accounting for updraft, downdraft, and entrainment mass fluxes for deep and shallow convection (Wu et al. 2007). Dry deposition in the model follows the standard resistance-in-series model of Wesely (1989). The wet deposition scheme includes scavenging of soluble tracer in convective updrafts, as well as rainout and washout of soluble tracers as described in Liu et al. (2001).

2.2 Emissions

Global emissions of reactive nitrogen oxides (NO_x), carbon monoxide (CO), sulfur dioxide (SO_2), and ammonia (NH_3) in the model are from the emission inventory in Task Force Hemispheric Transport of Air Pollution (HTAP, v2, 2008) (Janssens-Maenhout et al. 2015). The global emissions of non-methane volatile organic compounds (NMVOCs) are from the Global Emissions Inventory Activity (GEIA) inventory (Piccot et al. 1992). Global emissions of BC and OC follow Bond et al. (2007). The anthropogenic emissions of NO_x, CO, SO_2, NH_4, and NMVOCs in East Asia are overwritten by the MIX Asian anthropogenic emissions inventory of 2008 (Li et al. 2017). Biomass emissions are from the Global Fire Emissions Database-4 (GFED-4) inventory (Giglio et al. 2013).

2.3 Numerical experiments

To examine the effects of the chemical progress on summertime O_3 in UTLS over the TP/SASM region, we do simulations using the emissions and meteorological fields of 2008. The simulation year is chosen to be in accordance with the time period of the emissions (Sect. 2.2) and the observational data (Sect. 3). Following Eastham et al. (2014), we perform a 5-year spin-up run to generate the initial conditions so as to allow the stratospheric species to reach quasi-steady-state conditions.

3 Simulated and observed low O_3 concentration region

Observational and model studies have shown that the low O_3 concentration region exists in the UTLS (70–150 hPa) over the Tibetan Plateau during summertime (Liu et al. 2003; Bian et al. 2011; Gu et al. 2016). Figure 1a–d and Fig. 1e–h show the simulated and observed seasonal mean O_3 concentrations in March–April–May (MAM), June–July–August (JJA), September–October–November (SON), and December–January–February (DJF), respectively, in 2008. The observations are obtained from the Microwave Limb Sounder (MLS) version 3.3 level 2 products (ftp://acdisc.gsfc.nasa.gov/data/s4pa///Aura_MLS_Level2/). The MLS instrument aboard the Aura spacecraft has been providing valuable information on atmospheric parameters in the UTLS since August 2004 (Waters et al. 2006). Details of the MLS O_3 measurements were described in Livesey et al. (2011). Methods of data construction, screening and smoothing are similar to those in Gu et al. (2016).

Low O_3 mixing ratios of less than 180 ppbv over 10–40°N, 70–105°E could be seen in both the observations (Fig. 1f) and model simulations (Fig. 1b) in summer. As is shown in Fig. 1, the observed magnitude and distribution of O_3 mixing ratios (Fig. 1e–h) could be well captured by the GEOS-Chem UCX model (Fig. 1a–d) in all the seasons. Considering all the grid cells with MLS O_3 data available, the simulated and observed O_3 mixing ratios averaged over the TP/SASM region in JJA are 176.4 and 160.3 ppbv, respectively. The normalized mean bias (NMB) of the simulated seasonal mean O_3 concentrations at 100 hPa over the TP/SASM region is 11.8, 10.0, 4.4, and 9.9%, respectively, in MAM, JJA, SON, DJF. The NMB is defined as $\mathrm{NMB} = \frac{\sum_{i=1}^{n}(P_i - O_i)}{\sum_{i=1}^{n} O_i}$, where P_i and O_i are predicted and observed O_3 mixing ratios at grid i, n is the number of grids which have qualified observational data over the TP/SASM region.

In addition to the comparisons described above, the GEOS-Chem simulations of O_3 and its precursors have been evaluated for both the surface and the UTLS over the studied region in previous studies [Li et al. 2005 (UTLS CO); Eastham et al. 2014 (UTLS O_3 and NO_y); Gu et al. 2016 (surface and UTLS O_3)]. These studies showed that the GEOS-Chem model, especially the UCX, captured the magnitude and distributions of the UTLS O_3, CO and NO_y fairly well. The vertical distributions of O_3 over the Tibetan Plateau region have also been evaluated by balloon-borne sonde measurements in Kunming and Lhasa in Gu et al. (2016), showing that the model has the ability to reproduce the vertical profiles of O_3 in the studied region.

4 Chemical contributions to the UTLS O_3 concentrations in summer

Previous studies mostly focused on the physical contributions to the UTLS O_3 concentrations over the TP/SASM region during summertime (Fu et al. 2006; Randel and Park 2006; Park et al. 2007; Bian et al. 2011), pointing out that the low O_3 concentrations in the UTLS were caused by the deep convections that transported O_3-poor air upward from

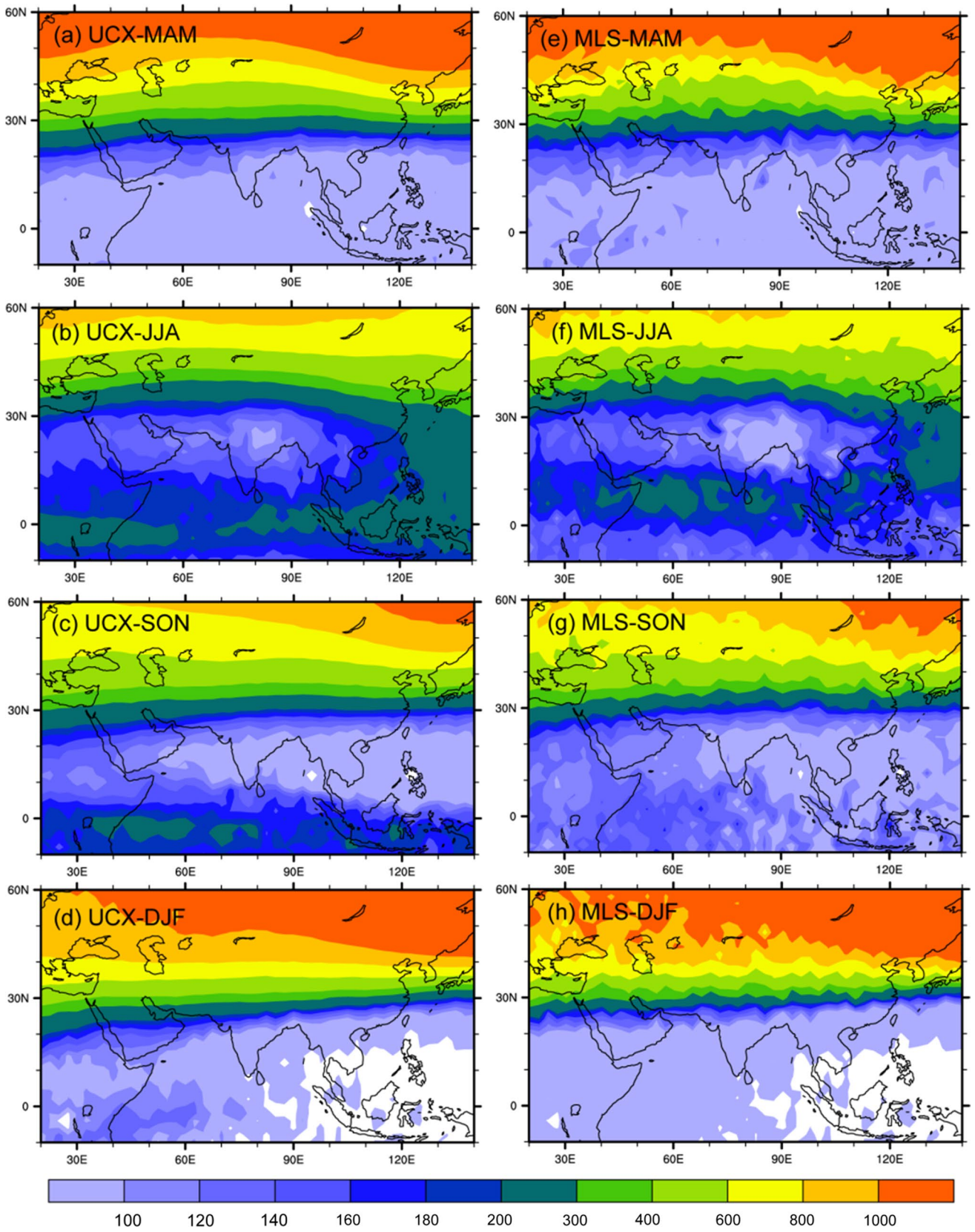

Fig. 1 Distributions of seasonal mean O_3 mixing ratios from UCX model result (**a**–**d**) and MLS observations (**e**–**h**) in MAM, JJA, SON, and DJF of 2008, units: ppbv. The simulated O_3 mixing ratios are smoothed by the satellite averaging kernels (same as Gu et al. 2016). White areas mean lake of data meeting the retrieval quality criteria

the lower troposphere. Few studies have investigated the role of the chemical processes in the formation of the low O_3 concentration region in boreal summer. By calculating the effects of physical and chemical processes on the changes of the average O_3 concentration at a selected grid point, Liu et al. (2003) indicated that the chemical effect was also important in the formation of low O_3 concentration region over the Tibetan Plateau in summer: the effect of the chemical process led an increase in O_3, which was opposite to that of the transport process. To compare with model results in Liu et al. (2003), we also calculate the contributions of net chemical production and the vertical transport to O_3 during April to July in the selected horizontal grid box of 31°N, 90°E. The net chemical production of O_3 (NP_{O_3}) is chemical production minus chemical loss calculated by the UCX model, including the effects of both the gas-phase reactions and the heterogeneous reactions such as the hydrolysis of N_2O_5 (Evans and Jacob 2005), irreversible absorption of NO_3 and NO_2 on wetted aerosol surfaces (Jacob 2000), and the uptake of HO_2 by aerosols (Thornton et al. 2008). The transport is the mass flux through the boundaries of the selected box. At 200 hPa, the contribution of NP_{O_3} in the selected box is 0.0086 Tg during April to July, which is comparable to the net transport effect (− 0.0159 Tg) during the same period. At 100 hPa, the vertical transport decreases the O_3 mass of the box by − 0.004 Tg period^{-1}, and the NP_{O_3} increase the O_3 mass by 0.001 Tg period^{-1}, the magnitude of the which is consistent with those in Liu et al. (2003).

To get a further view of the chemical effects on the UTLS O_3 over the TP/SASM region during summertime, Fig. 2 shows the simulated seasonal mean NP_{O_3} profiles in MAM, JJA, SON, and DJF of 2008 averaged over the TP/SASM region. All the NP_{O_3} profiles show positive values in the UTLS (200–70 hPa), indicating that chemical processes have an effect of increasing O_3 concentrations in the UTLS over the studied region. The profiles show peaks between 200 and 350 hPa as a result of high NO_x emissions from aircraft and lightning at those altitudes (Martin et al. 2007; Murray et al. 2012). In the UTLS, especially at altitudes above 350 hPa, NP_{O_3} in UTLS over the TP/SASM region is the largest in summer, indicating that there might be specific mechanisms that are conducive to the production of O_3 in UTLS during summertime. Figure 3 shows the seasonal mean distributions of NP_{O_3} in JJA of 2008. A remarkable feather in Fig. 3a is that the location of high NP_{O_3} region (0.016–0.020 Tg year^{-1}) is in accordance with that of low O_3 mixing ratios in Fig. 1b, f at 100 hPa. The region is also consistent with the location of the Tibetan anticyclone and that of the persistent maxima of other atmospheric constituents, such as NO_x (Park et al. 2004a), CO (Li et al. 2005; Park et al. 2007), C_2H_6 (Park et al. 2008). As for the latitude–altitude cross-section of the seasonal mean NP_{O_3} averaged over 70–105°E during summertime in Fig. 3b, high NP_{O_3} region

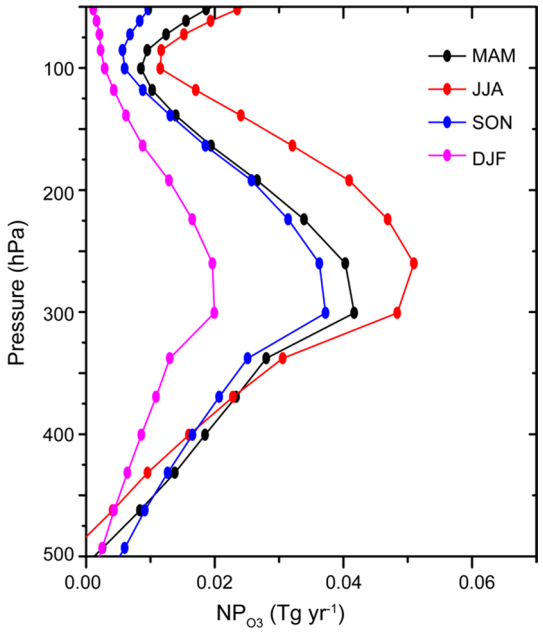

Fig. 2 Seasonal mean vertical distributions of NP_{O_3} (Tg year^{-1}) in MAM, JJA, SON, and DJF of 2008 averaged over the TP/SASM region

is simulated in the upper troposphere over the TP/SASM region, the maxima of which is at around 250 hPa, with a value of more than 0.06 Tg year^{-1}. The NP_{O_3} is negative in the middle troposphere, indicating that the depletion of O_3 is more than the production of O_3. This is a general trend of NP_{O_3} in line with previous discussions, which is due to the lowest NO_x concentrations in the middle troposphere (Bertsen and Isaksen 1997; Liu et al. 2003). By examining the seasonal variations of CO and NO_x at the grid point (31°N, 90°E, 100 hPa), Liu et al. (2003) indicated that the increasing NP_{O_3} might be attributed to the increase of NO_x and CO concentrations in corresponding regions. To further investigate the reasons of the enhancement of NP_{O_3} in the UTLS over TP/SASM, detailed discussions of the mechanisms for high NP_{O_3} over the studied region will be displayed in the following sections.

5 Mechanisms for high net chemical production of O_3 in the UTLS

Tropospheric O_3 is mainly produced by the photolysis of precursors (e.g. CO, VOCs, NO_x), and destroyed by the photolysis of O_3 and reaction with HO_x (Seinfeld and Pandis 2006). Thus, the concentrations of O_3 precursors, such as VOCs and NO_x, and the photolysis rates of O_3 and NO_2 determine whether ozone produces or consumes in the troposphere. To further investigate the reasons of the enhancement of NP_{O_3} in the UTLS over TP/SASM, we discuss the

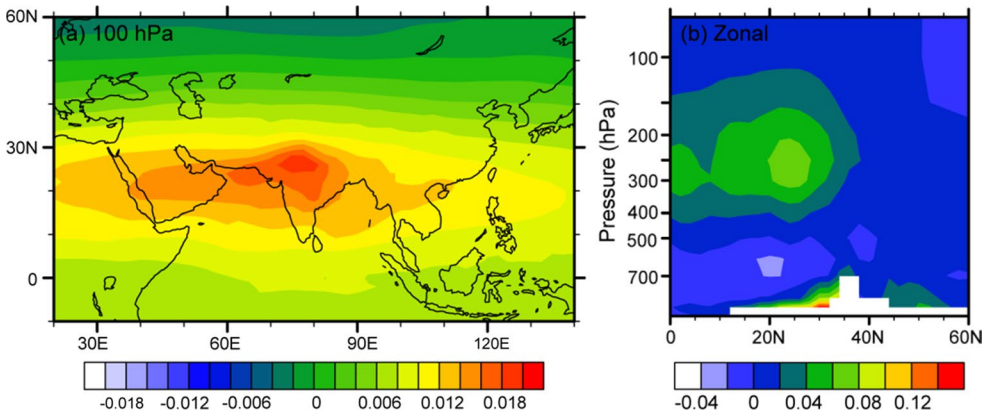

Fig. 3 The seasonal mean distributions of NP_{O_3} (Tg year^{-1}) during JJA of 2008 from UCX. **a** The simulated horizontal distributions of NP_{O_3} at 100 hPa, and **b** the latitude–altitude cross-section of simulated NP_{O_3} averaged over 70–105°E

dependence of O_3 production on the amount of precursors and the photolysis rates, respectively, in this section.

5.1 Dependence of O_3 production on the concentrations of precursors

Figure 4 shows the simulated horizontal distributions of NP_{O_3} and O_3 precursors (NO_x, VOCs, and CO) averaged over JJA of 2008 at 150, 200, and 300 hPa, respectively. At 300 hPa, the concentrations of NO_x (Fig. 4b), VOCs (Fig. 4c), and CO (Fig. 4d) show high values over Southern and Eastern Asia, consistent with sources from near-surface pollution and biomass burning (Streets et al. 2003; Zhang et al. 2009). As the altitude increases, the coverage of the high value region develops, exhibiting a distinct high value area over the TP/SASM region at 150 and 200 hPa. At 150 hPa, NO_x, VOCs, and CO show broad high values of ~ 0.5, ~ 4.5, and ~ 110 ppbv, respectively, in the TP/SASM region. Our simulations of NO_x and CO are in agreement with those reported in Park et al. (2004a) and Li et al. (2005). The former examined UTLS NO_x distributions from a 5-year sample of a long-term integration using the Halogen Occultation Experiment (HALOE) satellite observations and the Model for Ozone and Related Chemical Tracers (MOZART), reporting that the NO_x showed relative maxima of 0.5–0.6 ppbv at 158 hPa in July over 60–120°E, 10–40°N. The latter observed CO at 147 hPa in August and September 2004 using the MLS and MOPITT satellite, and the corresponding CO maximum over the TP/SASM region were ~ 130 and ~ 120 ppbv, respectively. Since observations of total VOCs over the studied region are limited, we compare our simulated C_2H_6 (not shown) with observations reported in Park et al. (2008). Simulated C_2H_6 show high values of 0.6–0.7 ppbv over the TP/SASM region at around 15 km during summertime, the magnitude of which is consistent with those observed in Park et al. (2008) during the Atmospheric Chemistry Experiment (ACE) in summer of 2004–2006.

Figure 4a displays the distributions of NP_{O_3} averaged over JJA of 2008 at 150, 200, and 300 hPa, respectively. Compared to Fig. 4b–d, the distributions of NP_{O_3} are similar to those of NO_x (Fig. 4b), VOCs (Fig. 4c), and CO (Fig. 4d), exhibiting high values of more than 0.05, 0.08, 0.10 Tg year^{-1} at 150, 200, and 300 hPa, respectively, over the TP/SASM region. The similarity between the distributions of NP_{O_3} in Fig. 4a and O_3 precursors in Fig. 4b–d can be quantified by the pattern correlation coefficient (PCC, http://glossary.ametsoc.org/wiki/Pattern_correlation). The PCCs between the distributions of NP_{O_3} and those of NO_x, VOCs, and CO over 60–120°E, 10–40°N (include TP/SASM defined in Sect. 1) at all the pressure levels are always above 0.9, indicating that the distribution of NP_{O_3} highly agrees with those of NO_x, VOCs, and CO over the studied region in summer. Park et al. (2008) measured the relative age of air by examining the ratio of C_2H_2/CO based on the measurements during the ACE mission in JJA of 2004–2006, suggesting relatively rapid transport of fresh emissions up to the UTLS over the TP/SASM region. Thus, as discussed in previous studies, the accumulation of CO (Kar et al. 2004; Li et al. 2005; Park et al. 2007), NO_x (Park et al. 2004a), and VOCs (Park et al. 2008) in the UTLS over the studied region due to the deep convection could be one important reason for the enhancement of NP_{O_3} in the UTLS over TP/SASM. The O_3 production rate is a function related with the ratio of VOCs and NO_x, and the VOCs/NO_x ratio could be used to identify whether a region is a 'NO_x-limited' or a 'VOCs-limited' region, so as to estimate different roles of NO_x and VOCs in the chemical production of O_3 (Sillman 1999, 2003). According to the model results, the calculated VOCs/NO_x ratios in most tropospheric regions over TP/SASM are larger than 10, which means that the studied region is a 'NO_x-limited' region, and the production of O_3 might be more sensitive to NO_x concentrations.

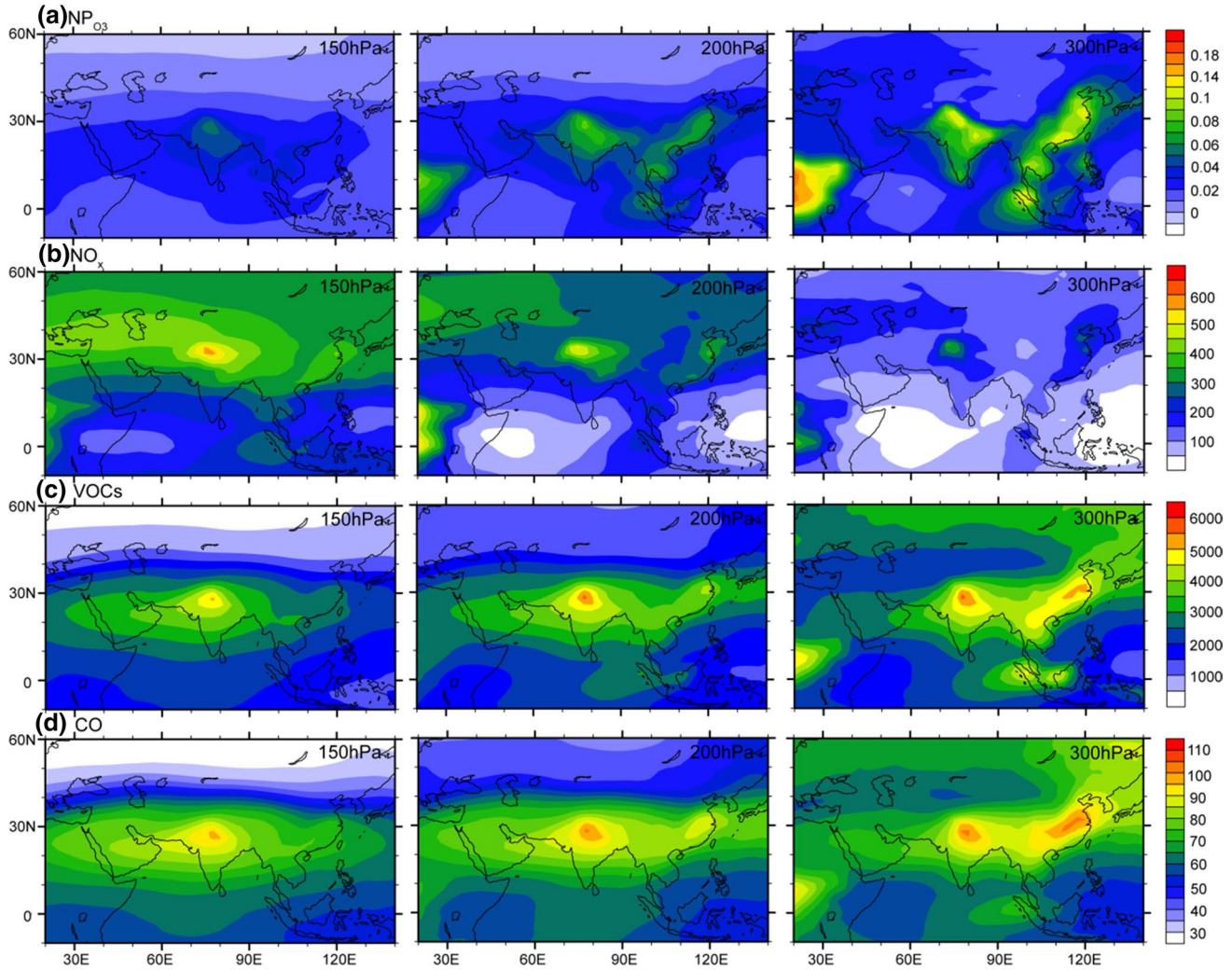

Fig. 4 Simulated distributions of NP_{O_3} (**a**) and O_3 precursors (**b**–**d**) averaged over JJA of 2008 at 150, 200, and 300 hPa, respectively. The unit of NP_{O_3} and CO is Tg year^{-1} and ppbv, respectively, while the units of NO_x ($NO_x = NO + NO_2$) and VOCs are pptv

5.2 Dependence of O_3 production on the photolysis rate

In addition to the concentrations of O_3 precursors, the photolysis rates of O_3 and NO_2 are also important in determining the values of NP_{O_3}. The photolysis rate of X could be defined as $r_X = J_X \times [X]$, where r_X [mol/(cm^3 s)] is the photolysis rate of X, $[X]$ (mol/cm^3) is the concentration of X, and J_X (s^{-1}) is the photolysis rate consistent (J values) of X (Seinfeld and Pandis 2006). Thus, J values together with species concentrations could be used to examine the photolysis rates of the corresponding species.

The J values vary greatly throughout the atmosphere, depending on atmospheric conditions such as overhead columns O_2 and O_3, solar zenith angle, pressure, temperature, aerosols and even clouds and surface albedo. Figure 5a shows the zonal mean distributions of NO_2 J values (J_{NO_2}) averaged over 70–105°E during JJA of 2008 from the UCX model. High values of J_{NO_2} are located at 100–300 hPa over 5–25°N with the range of 0.015–0.017 s^{-1}. The distributions of the high J values might result from the intense solar radiation in the tropical region and relatively less overhead O_3 column over the TP/SASM region during summer of the North Hemisphere (NH). The locations of high J_{NO_2} in Fig. 5a indicate that the J_{NO_2} are relatively high over TP/SASM, especially the SASM region (70–105°E, 10–25°N). According to HALOE observations in Park et al. (2004a) and our simulations, NO_2 concentrations also have high values in the UTLS over the TP/SASM region in summer as a result of the deep convection that transports NO_x-rich air upward from the lower troposphere. Since the photolysis rates of NO_2 is in proportion with NO_2 concentrations and J_{NO_2}, the photolysis rates of NO_2 could be high over the studied region and result in high chemical productions of

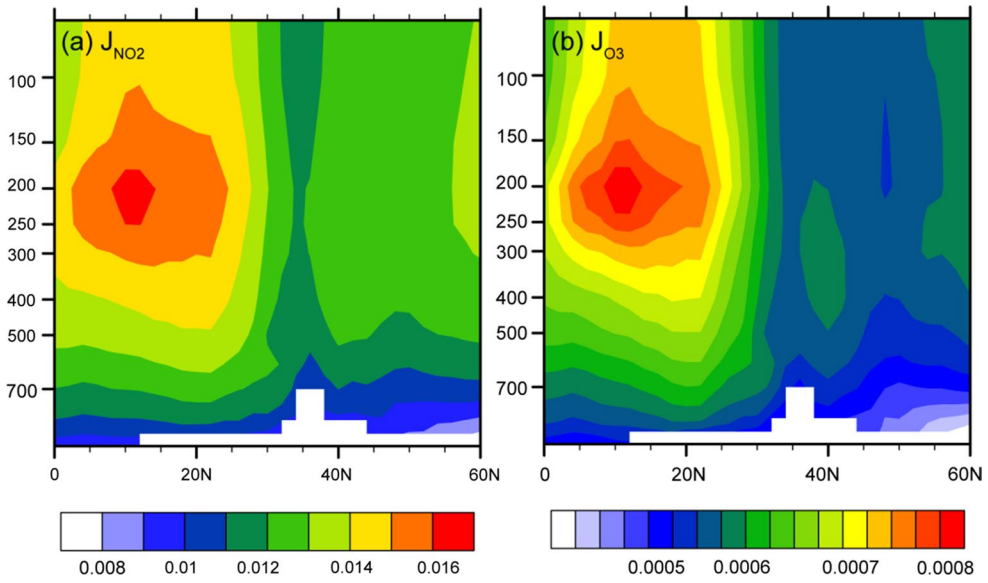

Fig. 5 The latitude–altitude cross section of *J* values of **a** NO_2, **b** and O_3 averaged over 70–105°E. The unit is S^{-1}, and all the data are averaged over JJA of 2008

O_3. In addition, Fig. 5b shows the zonal mean distributions of O_3 *J* values (J_{O_3}) averaged over 70–105°E during JJA of 2008 from the UCX model. J_{O_3} show similar distributions with J_{NO_2} over TP/SASM region, with high values located at 100–300 hPa in tropical and subtropical regions of NH. However, different from NO_2, O_3 concentrations show relatively low values over the TP/SASM region, which might weaken the positive contribution of J_{O_3} to the photolysis of O_3 to some extent.

Except for the convective transport of O_3 precursors from lower troposphere and active photochemistry in the middle and upper troposphere, there are other reasons that might contribute to the enhancement of NP_{O_3}. The UTLS over the TP/SASM region has been proved to be mostly effected by air masses from lower troposphere since tropospheric traces (e.g. CO, HCN, C_2H_6) exhibiting increased values (Park et al. 2008; Randel et al. 2010) while stratospheric tracers (e.g. O_3, HNO_3) exhibiting decreased values (Bian et al. 2011; Gu et al. 2016). Despite that, there are frequent stratosphere–troposphere exchanges that might bring elevated NO_x from the stratosphere and then contribute to the production of O_3 (Gettelman et al. 2011; Liang et al. 2011). In addition, NO_x released from intense lightning activities over the TP/SASM region during summertime could also enhance the formation of O_3 in the middle and upper troposphere. By analyzing the difference between simulations with and without lightning using the ECHAM5-HAMMOZ model, Fadnavis et al. (2015) indicated that the intense convections during summertime over the Asian summer monsoon regions were associated with frequent lightning activities which thereby result in the formation of additional NO_x. However, sensitivity results of their study showed that the contribution of lightning to NO_x in the UTLS over the TP/SASM region was much lower than that of anthropogenic emissions. The aerosol layer over the studied region, as reported in previous studies (Gu et al. 2016), could also affect NP_{O_3} by heterogeneous reactions and altering photolysis rates. Lou et al. (2014) reported that the combined impacts of aerosols could lead to 8–24% reductions in O_3 concentrations in China, indicating that the presence of the aerosol layer could not result in the enhancement of NP_{O_3}.

6 Conclusion

In this work, we simulate O_3 and its chemical production in the UTLS over the TP/SASM region during summertime in 2008, using the global chemical transport model GEOS-Chem with the UCX mechanism driven by the assimilated meteorological fields.

The model's ability to simulate UTLS O_3 is evaluated in all the seasons over the studied region. At 100 hPa, the distributions of simulated O_3 agree well with the MLS measurements. Both simulated and observed O_3 concentrations show low O_3 values of less than 180 ppbv at 100 hPa over the TP/SASM region. The simulated seasonal mean O_3 concentrations over the TP/SASM region show NMBs of 11.8, 10.0, 4.4, and 9.9%, respectively, in MAM, JJA, SON, DJF at 100 hPa, and the model biases lie within the confidence range of the MLS instruments.

The contributions of net chemical production and the vertical transport to O_3 during April to July are calculated in the selected horizontal grid box of 31°N, 90°E so as to make comparisons with model results in Liu et al. (2003). The effect of the chemical processes leads an increase in O_3, which is opposite to that of the transport process. At 200 hPa, NP_{O_3} in the selected box is 0.0086 Tg during April to July, which is comparable to the net effect of transport

(− 0.0159 Tg) during the same period. NP_{O_3} values in UTLS over the TP/SASM region are the largest in summer. The location of high NP_{O_3} region is in accordance with that of low O_3 mixing ratios at 100 hPa, and is also consistent with the location of the Tibetan anticyclone and those of the persistent maxima of other atmospheric constituents.

The enhancement of concentrations of O_3 precursors (e.g. NO_x, VOCs, and CO) and the active photochemical activities of NO_2 in the UTLS over the TP/SASM region during summertime could be important reasons for the enhancement of NP_{O_3} over the studied region. At 300 hPa, the simulated locations of high concentrations of NO_x, VOCs, and CO are consistent with sources from near-surface pollution and biomass burning. The coverage of the high value region develops as the altitude increases, exhibiting a distinct high value area over the TP/SASM region at 150 and 200 hPa. The distribution of NP_{O_3} highly agrees with that of NO_x, VOCs, and CO over the studied region, with PCCs larger than 0.9 at all the pressure levels over 60–120°E, 10–40°N. The results indicate that the accumulation of CO, NO_x, and VOCs could be one important reason for the enhancement of NP_{O_3} in the UTLS over TP/SASM in summer. In addition, both the concentrations and J values of NO_2 have high values in the UTLS over the TP/SASM region in summer, which lead to high photolysis rates of NO_2 over the studied region and then result in high chemical production of O_3.

Acknowledgements This work was supported by the Science and Technology Commission of Shanghai (Grant No. 16DZ1204607), the National Natural Science Foundation of China (Grant Nos. 91644223, 91637101, and 91744311), and the Shanghai Meteorological Service (Grant No. QM2017015). We gratefully acknowledge NASA, United States, for providing the MLS data on their website.

References

Alexander B, Park RJ, Jacob DJ, Li Q, Yantosca RM, Savarino J, Lee C, Thiemens M (2005) Sulfate formation in sea-salt aerosols: constraints from oxygen isotopes. J Geophys Res 110:D10307. https://doi.org/10.1029/2004JD005659

Alexander LV, Allen SK, Bindoff NL et al (2007) Climate change 2013: the physical science basis, in contribution of Working Group I (WGI) to the Fifth Assessment Report (AR5) of the Intergovernmental Panel on Climate Change (IPCC). Cambridge University Press, Cambridge

Bertsen TK, Isaksen SA (1997) A global three-dimensional chemical transport model for the troposphere: 1. Model description and CO and ozone results. J Geophys Res 102(D17):21239–21280. https://doi.org/10.1029/97JD01140

Bey I, Jacob DJ, Yantosca RM, Logan JA, Field B, Fiore AM, Li Q, Liu H, Mickley LJ, Schultz M (2001) Global modeling of tropospheric chemistry with assimilated meteorology: model description and evaluation. J Geophys Res 106(D19):23073–23095. https://doi.org/10.1029/2001JD000807

Bian J, Yan R, Chen H, Lü D, Massie ST (2011) Formation of the summertime ozone valley over the tibetan plateau: the Asian summer monsoon and air column variations. Adv Atmos Sci 28(6):1318–1325. https://doi.org/10.1007/s00376-011-0174-9

Bond TC, Bhardwaj E, Dong R, Jogani R, Jung SK, Roden C, Streets DG, Trautmann NM (2007) Historical emissions of black and organic carbon aerosol from energy-related combustion, 1850–2000. Global Biogeochem Cycles 21(2):GB2018. https://doi.org/10.1029/2006gb002840

Eastham SD, Weisenstein DK, Barret SRH (2014) Development and evaluation of the unified tropospheric-stratospheric chemistry extension (UCX) for the global chemistry-transport model GEOS-Chem. Atmos Environ 89:52–63. https://doi.org/10.1016/j.atmosenv.2014.02.001

Evans MJ, Jacob DJ (2005) Impact of new laboratory studies of N_2O_5 hydrolysis on global model budgets of tropospheric nitrogen oxides, ozone, and OH. Geophys Res Lett 32:L09813. https://doi.org/10.1029/2005GL022469

Fadnavis S, Semeniuk K, Schultz MG, Kiefer M, Mahajan A, Pozzoli L, Sonbawane S (2015) Transport pathways of peroxyacetyl nitrate in the upper troposphere and lower stratosphere from different monsoon systems during the summer monsoon season. Atmos Chem Phys 15:11477–11499. https://doi.org/10.5194/acp-15-11477-2015

Fairlie TD, Jacob DJ, Park RJ (2007) The impact of transpacific transport of mineral dust in the United States. Atmos Environ 41:1251–1266. https://doi.org/10.1016/j.atmosenv.2006.09.048

Fann N, Lamson AD, Anenberg SC, Wesson K, Risley D, Hubbell BJ (2012) Estimating the national public health burden associated with exposure to ambient $PM_{2.5}$ and ozone. Risk Anal 32:81–95. https://doi.org/10.1111/j.1539-6924.2011.01630.x

Fountoukis C, Nenes A (2007) ISORROPIA II: a computationally efficient thermodynamic equilibrium model for K^+–Ca^{2+}–Mg^{2+}–NH_4^+–Na^+–SO_4^{2-}–NO_3^-–Cl–H_2O aerosols. Atmos Chem Phys 7:4639–4659. https://doi.org/10.5194/acp-7-4639-2007

Fu R, Hu Y, Wright JS, Jiang JH, Dickinson RE, Chen M, Filipiak M, Read WG, Waters JW, Wu DL (2006) Short circuit of water vapor and polluted air to the global stratosphere by convective transport over the Tibetan Plateau. Proc Natl Acad Sci USA 103:5664–5669. https://doi.org/10.1073/pnas.0601584103

Gettelman A, Kinnison DE, Dunkerton TJ, Brasseur GP (2004) Impact of monsoon circulations on the upper troposphere and lower stratosphere. J Geophys Res 109:D22101. https://doi.org/10.1029/2004JD004878

Gettelman A, Hoor P, Pan LL, Randel WJ, Hegglin MI, Birner T (2011) The extratropical upper troposphere and lower stratosphere. Rev Geophys 49:RG3003. https://doi.org/10.1029/2011rg000355

Giglio L, Randerson JT, van der Werf GR (2013) Analysis of daily, monthly, and annual burned area using the fourth-generation global fire emissions database (GFED4). J Geophys Res 118:317–328. https://doi.org/10.1002/jgrg.20042

Gu Y, Liao H, Bian J (2016) Summertime nitrate aerosol in the upper troposphere and lower stratosphere over the Tibetan Plateau and the South Asian summer monsoon region. Atmos Chem Phys 16:6641–6663. https://doi.org/10.5194/acp-16-6641-2016

Hack JJ (1994) Parameterization of moist convection in the National Center for Atmospheric Research community climate model (CCM2). J Geophys Res 99:5551–5568. https://doi.org/10.1029/93jd03478

Jacob DJ (2000) Heterogeneous chemistry and tropospheric ozone. Atmos Environ 34:2131–2159

Jaeglé L, Quinn P, Bates T, Alexander B, Lin JT (2011) Global distribution of sea salt aerosols: new constraints from in situ and remote sensing observations. Atmos Chem Phys 11:3137–3157. https://doi.org/10.5194/acp-11-3137-2011

Janssens-Maenhout G, Crippa M, Guizzardi D, Dentener F, Muntean M, Pouliot G, Keating T, Zhang Q, Kurokawa J, Wankmüller R, van der Gon HD, Kuenen JJP, Klimont Z, Frost G, Darras S,

Koffi B, Li M (2015) Htap_v2.2: a mosaic of regional and global emission grid maps for 2008 and 2010 to study hemispheric transport of air pollution. Atmos Chem Phys 15(8):12867–12909. https://doi.org/10.5194/acp-15-11411-2015

Kar J, Bremer H, Drummond JR, Rochon YJ, Jones D, Nichitiu F, Zou J, Liu J, Gille JC, Edwards DP (2004) Evidence of vertical transport of carbon monoxide from Measurements of Pollution in the Troposphere (MOPITT). Geophys Res Lett 31:L23105. https://doi.org/10.1029/2004GL021128

Lau KM, Kim MK, Kim KM (2006) Asian summer monsoon anomalies induced by aerosol direct forcing: the role of the Tibetan Plateau. Clim Dyn 26:855–864. https://doi.org/10.1007/s00382-006-0114-z

Lawrence MG, Lelieveld J (2010) Atmospheric pollutant outflow from southern Asia: a review. Atmos Chem Phys 10:11017–11096. https://doi.org/10.5194/acp-10-11017-2010

Li Q, Jiang JH, Wu DL, Read WG, Livesey NJ, Waters JW, Zhang Y, Wang B, Filipiak MJ, Davis CP (2005) Convective outflow of South Asian pollution: a global CTM simulation compared with EOS MLS observations. Geophys Res Lett 32:L14826. https://doi.org/10.1029/2005GL022762

Li M, Zhang Q, Kurokawa JI, Woo JH, He K, Lu Z, Ohara T, Song Y, Streets DG, Carmichael GR, Cheng Y, Hong C, Huo H, Jiang X, Kang S, Liu F, Su H, Zheng B (2017) MIX: a mosaic Asian anthropogenic emission inventory under the international collaboration framework of the MICS-Asia and HTAP. Atmos Chem Phys 17:935–963. https://doi.org/10.5194/acp-17-935-2017

Liang Q, Rodriguez JM, Douglass AR, Crawford JH, Olson JR, Apel E, Bian H, Blake DR, Brune W, Chin M, Colarco PR, da Silva A, Diskin GS, Duncan BN, Huey LG, Knapp DJ, Montzka DD, Nielsen JE, Pawson S, Riemer DD, Weinheimer AJ, Wisthaler A (2011) Reactive nitrogen, ozone and ozone production in the Arctic troposphere and the impact of stratosphere-troposphere exchange. Atmos Chem Phys 11:13181–13199. https://doi.org/10.5194/acp-11-13181-2011

Liu H, Jacob DJ, Bey I, Yantosca RM (2001) Constraints from ^{210}Pb and ^{7}Be on wet deposition and transport in a global three-dimensional chemical tracer model driven by assimilated meteorological fields. J Geophys Res 106:12109–12128. https://doi.org/10.1029/2000JD900839

Liu Y, Li W, Zhou X, He J (2003) Mechanism of formation of the ozone valley over the Tibetan Plateau in summer-transport and chemical process of ozone. Adv Atmos Sci 20(1):103–109

Livesey NJ, Read WG, Wagner PA, Froidevaux L, Lambert A, Manney GL, Pumphrey HC, Santee ML, Schwartz MJ, Wang S, Cofield RE, Cuddy DT, Fuller RA, Jarnot RF, Jiang JH, Knosp BW (2011) Earth Observing System (EOS) Microwave Limb Sounder (MLS) Version 3.3 Level 2 data quality and description document. Tech Rep JPL D-33509, NASA Jet Propulsion Laboratory. http://mls.jpl.nasa.gov/data/v3-3_data_quality_document.pdf

Logan JA, Megretskaia IA, Miller AJ, Tiao GC, Choi D, Zhang L, Stolariski RS, Labow GJ, Hollandsworth SM, Bodeker GE, Claude H, De Muer D, Kerr JB, Tarasick DW, Oltmans SJ, Johnson B, Schmidlin F, Staehelin J, Viatte P, Uchino O (1999) Trends in the vertical distribution of ozone: a comparison of two analyses of ozonesonde data. J Geophys Res 104(D21):26373–26399. https://doi.org/10.1029/1999JD900300

Lou S, Liao H, Zhu B (2014) Impacts of aerosols on surface-layer ozone concentrations in China through heterogeneous reactions and changes in photolysis rates. Atmos Environ 85:123–138. https://doi.org/10.1016/j.atmosenv.2013.12.004

Martin RV, Sauvage B, Folkins I, Sioris CE, Boone C, Bernath P, Ziemke J (2007) Space-based constraints on the production of nitric oxide by lightning. J Geophys Res 112:D09309. https://doi.org/10.1029/2006JD007831

McConnell JC, Jin JJ (2008) Stratospheric ozone chemistry. Atmos Ocean 46(1):69–92. https://doi.org/10.3137/ao.460104

Murray LT, Jacob DJ, Logan JA, Hudman RC, Koshak WJ (2012) Optimized regional and interannual variability of lightning in a global chemical transport model constrained by LIS/OTD satellite data. J Geophys Res 117:D20307. https://doi.org/10.1029/2012JD017934

Oltmans SJ, Lefohn AS, Scheel HE, Harris JM, Levy H II, Gallbally IE, Brunke EG, Meyer CP, Lanthrop JA, Hohnson BJ, Shadwick DS, Cuevas E, Schmidlin FJ, Tarasick DW, Claude H, Kerr JB, Uchino O, Mohnen V (1998) Trends of ozone in the troposphere. Geophys Res Lett 25:139–142

Park M, Randel WJ, Kinnison DE, Garcia RR, Choi W (2004a) Seasonal variation of methane, water vapor, and nitrogen oxides near the tropopause: satellite observations and model simulations. J Geophys Res 109:D03302. https://doi.org/10.1029/2003JD003706

Park RJ, Jacob DJ, Field BD, Yantosca RM, Chin M (2004b) Natural and transboundary pollution influences on sulfate–nitrate–ammonium aerosols in the United States: implications for policy. J Geophys Res 109:D15204. https://doi.org/10.1029/2003JD004473

Park M, Randel WJ, Gettelman A, Massie ST, Jiang JH (2007) Transport above the Asian summer monsoon anticyclone inferred from Aura Microwave Limb Sounder tracers. J Geophys Res 112:D16309. https://doi.org/10.1029/2006JD008294

Park M, Randel WJ, Emmons LK, Bernath PF, Walker KA, Boone CD (2008) Chemical isolation in the Asian monsoon anticyclone observed in Atmospheric Chemistry Experiment (ACE-FTS) data. Atmos Chem Phys 8:757–764. https://doi.org/10.5194/acp-8-757-2008

Piccot SD, Watson JJ, Jones JW (1992) A global inventory of volatile organic compound emissions from anthropogenic sources. J Geophys Res 97:9897–9912. https://doi.org/10.1029/92JD00682

Pye H, Liao H, Wu S, Mickley LJ, Jacob DJ, Henze DK, Seinfeld J (2009) Effect of changes in climate and emissions on future sulfate–nitrate–ammonium aerosol levels in the United States. J Geophys Res 114:D01205. https://doi.org/10.1029/2008JD010701

Randel WJ, Park M (2006) Deep convective influence on the Asian summer monsoon anticyclone and associated tracer variability observed with Atmospheric Infrared Sounder (AIRS). J Geophys Res 111:D12314. https://doi.org/10.1029/2005JD006490

Randel WJ, Park M, Emmons L, Kinnison D, Bernath P, Walker KA, Boone C, Pumphrey H (2010) Asian monsoon transport of pollution to the stratosphere. Science 328:611–613. https://doi.org/10.1126/science.1182274

Rao TN, Kirkwood S, Arvelius J, von der Gathen P, Kivi R (2003) Climatology of UTLS ozone and the ratio of ozone and potential vorticity over northern Europe. J Geophys Res 108(D22):4703. https://doi.org/10.1029/2003JD003860

Rotman DA, Tannahill JR, Kinnison DE, Connell PS, Bergmann D, Proctor D, Rodriguez JM, Lin SJ, Rood RB, Prather MJ, Rasch PJ, Considine DB, Ramaroson R, Kawa SR (2001) Global modeling initiative assessment model: model description, integration, and testing of the transport shell. J Geophys Res 106:1669–1691

Sander SP, Friedl RR, Barker JR, Golden DM, Kurylo MJ, Sciences GE, Wine PH, Abbatt JPD, Burkholder JB, Kolb CE, Moortgat GK, Huie RE, Orkin VL (2011) Chemical Kinetics and Photochemical Data for Use in Atmospheric Studies Evaluation Number 17 NASA Panel for Data Evaluation. JPL Publications. http://pubman.mpdl.mpg.de/pubman/faces/viewItemFullPage.jsp?itemId=escidoc%3A1827926%3A1

Seinfeld JH, Pandis SN (2006) Atmospheric chemistry and physics: from air pollution to climate change, 2nd edn. Wiley-Interscience, New York

Shindell D, Kuylenstierna JCI, Vignati E, van Dingenen R, Amann M, Klimont Z, Anenberg SC, Muller N, Janssens-Maenhout G, Raes F, Schwartz J, Faluvegi G, Pozzoli L, Kupiainen K, Höglund-Isaksson L, Emberson L, Streets D, Ramanathan V, Hicks K,

Oanh NTK, Milly G, Williams M, Demkine V, Fowler D (2012) Simultaneously mitigating near-term climate change and improving human health and food security. Science 335(6065):183–189. https://doi.org/10.1126/science.1210026

Sillman S (1999) The relation between ozone, NO_x and hydrocarbons in urban and polluted rural environments. Millenial Review series. Atmos Environ 33(12):1821–1845

Sillman S (2003) Tropospheric ozone and photochemical smog. In: Lollar BS (ed) Treatise on geochemistry. Elsevier, Amsterdam, pp 407–431

Staehelin J, Harris NRP, Appenzeller C, Eberhard J (2001) Ozone trends: a review. Rev Geophys 39(2):231–290. https://doi.org/10.1029/1999RG000059

Streets DG, Bond TC, Carmichael GR, Fernandes SD, Fu Q, He D, Klimont Z, Nelson SM, Tsai NY, Wang MQ, Woo JH, Yarber KF (2003) An inventory of gaseous and primary aerosol emissions in Asia in the year 2000. J Geophys Res 108(D21):8809. https://doi.org/10.1029/2002JD003093

Thornton JA, Jaegle L, McNeill VF (2008) Assessing known pathways for HO_2 loss in aqueous atmospheric aerosols: regional and global impacts on tropospheric oxidants. J Geophys Res 113:D05303. https://doi.org/10.1029/2007JD009236

Tian W, Chipperfield M, Huang Q (2008) Effects of the Tibetan Plateau on total column ozone distribution. Tellus 60(4):622–635. https://doi.org/10.1111/j.1600-0889.2008.00338.x

Tobo Y, Iwasaka Y, Zhang D, Shi D, Kim YS, Tamura K, Ohashi T (2008) Summertime "ozone valley" over the Tibetan Plateau derived from ozonesondes and EP/TOMS data. Geophys Res Lett 35:L16801. https://doi.org/10.1029/2008GL034341

Waters JW, Froidevaux L, Harwood RS, Jarnot RF, Pickett HM, Read WG, Siegel PH, Cofield RE, Filipiak MJ, Flower D (2006) The earth observing system microwave limb sounder (EOS MLS) on the Aura satellite. IEEE Trans Geosci Remote 44(5):1075–1092. https://doi.org/10.1109/TGRS.2006.873771

Wesely M (1989) Parameterization of surface resistances to gaseous dry deposition in regional-scale numerical models. Atmos Environ 23(6):1293–1304. https://doi.org/10.1016/0004-6981(89)90153-4

Wild O, Zhu X, Prather MJ (2000) Fast-J: accurate simulation of in- and below-cloud photolysis in tropospheric chemical models. J Atmos Chem 37(3):245–282. https://doi.org/10.1023/A:1006415919030

Wu S, Mickley LJ, Jacob DJ, Logan JA, Yantosca RM, Rind D (2007) Why are there large differences between models in global budgets of tropospheric ozone? J Geophys Res 112:D05302. https://doi.org/10.1029/2006JD007801

Xia X, Zong X, Cong Z, Chen H, Kang S, Wang P (2011) Baseline continental aerosol over the central Tibetan plateau and a case study of aerosol transport from South Asia. Atmos Environ 45(39):7370–7378. https://doi.org/10.1016/j.atmosenv.2011.07.067

Yue X, Unger N (2014) Ozone vegetation damage effects on gross primary productivity in the United States. Atmos Chem Phys 14:9137–9153. https://doi.org/10.5194/acp-14-9137-2014

Zhang GJ, McFarlane NA (1995) Sensitivity of climate simulations to the parameterization of cumulus convection in the Canadian Climate Centre general circulation model. Atmos Ocean 33:407–446. https://doi.org/10.1080/07055900.1995.9649539

Zhang Q, Streets DG, Carmichael GR, He KB, Huo H, Kannari A, Klimont Z, Park IS, Reddy S, Fu JS, Chen D, Duan L, Lei Y, Wang LT, Yao ZL (2009) Asian emissions in 2006 for the NASA INTEX-B mission. Atmos Chem Phys 9:5131–5153. https://doi.org/10.5194/acp-9-5131-2009

Zhou X, Li W, Chen L, Liu Y (2006) Study on ozone change over the Tibetan Plateau. Acta Meteorol Sin 20(2):129–143